

Tail Emission of Prompt Gamma-Ray Burst Jets

Ryo Yamazaki¹, Kenji Toma², Kunihito Ioka², and Takashi Nakamura²

¹*Department of Earth and Space Science, Osaka University, Toyonaka 560-0043, Japan*

²*Department of Physics, Kyoto University, Kyoto 606-8502, Japan*

ryo@vega.ess.sci.osaka-u.ac.jp, toma@tap.scphys.kyoto-u.ac.jp,
ioka@tap.scphys.kyoto-u.ac.jp, takashi@tap.scphys.kyoto-u.ac.jp

ABSTRACT

Tail emission of the prompt gamma-ray burst is discussed using a multiple emitting sub-shell (inhomogeneous jet, sub-jets) model. The tail is a superposition of a number of smooth, long-duration, dim, and soft pulses emitted by segments located far from the line of sight. We find that the behavior of the tail is not so much affected by the local inhomogeneity but affected by the global sub-jet distribution. Some observed tails may disfavor the power-law jets.

Subject headings: gamma rays: bursts — gamma rays: theory

1. Introduction

Gamma-ray bursts (GRBs) consist of two phases: prompt GRB emission and subsequent afterglows. How long the prompt GRB emission lasts and when the transition from the prompt GRB to the afterglow occurs have been long-standing problems. These problems are tightly related to the mechanism of the central engine of GRBs. In general, the prompt GRB tends to show a spectral softening and a rapid decay (e.g., Giblin et al. 1999; Connaughton 2002), so that the X-ray observation with high flux sensitivity is necessary to investigate the end epoch of the prompt GRB. Such an observation has become possible thanks to the *Swift* satellite, which are revealing rich structures in early X-ray counterparts of GRBs (Burrows et al. 2005; Chincarini et al. 2005; Campana et al. 2005; Tagliaferri et al. 2005; Nousek et al. 2005). A distinct decaying component before the usual afterglow phase is identified. During this epoch, the decay is steeper and the spectral index is different compared with the subsequent phase (Nousek et al. 2005). These results suggest that this component is the tail emission of the prompt GRB (Zhang et al. 2005; Panaitescu et al. 2005).

Most natural explanation for the tail is a high latitude emission from a relativistically moving shell (Kumar & Panaitescu 2000; Yamazaki et al. 2005). Suppose the shell shines for

a short period. Since the shell has a curvature, photons far from the line of sight come later. Because the shell at higher latitude from the line of sight has a lower velocity toward the observer, the emission becomes dimmer and softer as time passes because of the relativistic beaming effect. For a spherical uniform shell, the predicted decay index is around -3 (Kumar & Panaitescu 2000), while events with more rapid decay exist (Nousek et al. 2005). Since the emission region sweeps the shell, the tail emission features, e.g., the decay index and smoothness, would diagnose the unknown GRB jet structure.

Swift observations show a diversity of early X-ray afterglow light curves, which might be ascribed to the angular inhomogeneity of GRB jets. In this paper, we discuss the tail emission of the structured inhomogeneous GRB jets by using a multiple emitting sub-shell (inhomogeneous jet, sub-jets) model considered so far (Nakamura 2000; Kumar & Piran 2000; Yamazaki, Ioka, & Nakamura 2004b; Toma, Yamazaki, & Nakamura 2005a,b). Our model well reproduces the observed features of the tail emission of the prompt GRB. This paper is organized as follows. In § 2, we briefly introduce our prompt emission model. The tail emission of GRB is discussed in § 3. Section 4 is devoted to discussions.

2. Prompt emission model

We consider the same model as discussed in our previous works (Yamazaki, Ioka, & Nakamura 2004b; Toma, Yamazaki, & Nakamura 2005a,b). The whole GRB jet, whose opening half-angle is $\Delta\theta_{\text{tot}}$, consists of N_{tot} emitting sub-shells (sub-jets) (Nakamura 2000; Kumar & Piran 2000). We introduce the spherical coordinate system $(r, \vartheta, \varphi, t)$ in the central engine frame, where the origin is at the central engine, and $\vartheta = 0$ is the axis of the whole jet. Each sub-jet departs at time $t_{\text{dep}}^{(j)}$ ($0 < t_{\text{dep}}^{(j)} < t_{\text{dur}}$, where $j = 1, \dots, N_{\text{tot}}$, and t_{dur} is the active time of the central engine) from the central engine in the direction of $\vec{n}^{(j)} = (\vartheta^{(j)}, \varphi^{(j)})$. The direction of the observer is denoted by $\vec{n}_{\text{obs}} = (\vartheta_{\text{obs}}, \varphi_{\text{obs}})$. For each sub-jet, the emission model is the same as in the previous works (Granot, Piran, & Sari 1999; Woods & Loeb 1999; Ioka & Nakamura 2001; Yamazaki, Ioka, & Nakamura 2002, 2003, 2004a). The observed flux from the j th sub-jet is calculated when the following parameters are determined: the viewing angle of the sub-jet $\theta_v^{(j)} = \cos^{-1}(\vec{n}_{\text{obs}} \cdot \vec{n}^{(j)})$, the opening half-angle of the sub-jet $\Delta\theta_{\text{sub}}^{(j)}$, the departure time $t_{\text{dep}}^{(j)}$, the Lorentz factor $\gamma^{(j)} = (1 - \beta_{(j)}^2)^{-1/2}$, the emitting radius $r_0^{(j)}$, the low- and high-energy photon index $\alpha_B^{(j)}$ and $\beta_B^{(j)}$, the break frequency in the shell comoving frame $\nu_0^{\prime(j)}$ (Band et al. 1993), the normalization constant of the emissivity $A^{(j)}$, and the source redshift z . The whole light curve from the GRB jet is produced by the superposition of the sub-jet emission. Throughout the paper, we neglect the cosmological effect, i.e., we set $z = 0$.

As we will see later, local inhomogeneities in our model are almost averaged during the tail emission phase, and the global jet structure (the mean sub-jet distribution) determines the decay index of the tail. Therefore, essentially we are also studying the tail emission from the usual structured jets at once, i.e., from uniform or power-law jets with no local inhomogeneity.

3. Tail Emission of Prompt GRB

3.1. General Kinematical Considerations

We present some of kinematical properties of prompt GRBs in the multiple sub-jet model. Let $\theta_v^{(j)}$ be the angle between the observer's line of sight and the axis of the j th sub-jet. The pulse starting and ending time at the observer are given by

$$T_{\text{start}}^{(j)} \sim t_{\text{dep}}^{(j)} + \frac{r_0^{(j)}}{2c\gamma_{(j)}^2} \left(1 + \gamma_{(j)}^2 \theta_-^{(j)2}\right) , \quad (1)$$

$$T_{\text{end}}^{(j)} \sim t_{\text{dep}}^{(j)} + \frac{r_0^{(j)}}{2c\gamma_{(j)}^2} \left(1 + \gamma_{(j)}^2 \theta_+^{(j)2}\right) , \quad (2)$$

where $\theta_+^{(j)} = \theta_v^{(j)} + \Delta\theta_{\text{sub}}^{(j)}$ and $\theta_-^{(j)} = \max\{0, \theta_v^{(j)} - \Delta\theta_{\text{sub}}^{(j)}\}$, and we use the formulae $\beta_{(j)} \sim 1 - 1/2\gamma_{(j)}^2$ and $\cos\theta \sim 1 - \theta^2/2$ for $\gamma^{(j)} \gg 1$ and $\theta \ll 1$, respectively. Then, the pulse duration, $\delta T^{(j)} = T_{\text{end}}^{(j)} - T_{\text{start}}^{(j)}$, is given by $\delta T^{(j)} \sim 1.5 r_{14}(\theta_+^{(j)}/0.03)^2$ s for $\theta_v^{(j)} < \Delta\theta_{\text{sub}}^{(j)}$, and

$$\delta T^{(j)} \sim 26 r_{14}(\Delta\theta_{\text{sub}}^{(j)}/0.02)(\theta_v^{(j)}/0.2) \text{ sec} , \quad (3)$$

for $\theta_v^{(j)} > \Delta\theta_{\text{sub}}^{(j)}$, where $r_{14} = r_0^{(j)}/10^{14}$ cm. The peak energy $E_p^{(j)}$, that gives the peak of the νF_ν spectrum, is approximated as $E_p^{(j)} \propto \nu_0'^{(j)} \delta^{(j)}$, where $\delta^{(j)} = [\gamma^{(j)}(1 - \beta_{(j)} \cos\theta_-^{(j)})]^{-1}$. Using practical numerical calculations, we find $E_p^{(j)} \approx 6.5 \times 10^2 \gamma_2 \nu_5$ keV for $\theta_v^{(j)} \ll \Delta\theta_{\text{sub}}^{(j)}$, and

$$E_p^{(j)} \approx 2 \gamma_2^{-1} \nu_5 (\theta_v^{(j)}/0.2)^{-2} \text{ keV} , \quad (4)$$

for $\theta_v^{(j)} \gg \Delta\theta_{\text{sub}}^{(j)}$, where $\nu_5 = \nu_0'^{(j)}/5$ keV and $\gamma_2 = \gamma^{(j)}/10^2$. We note that the light curve from a single pulse becomes dim and smooth for large $\theta_v^{(j)}$ (see Fig. 2 of Ioka & Nakamura 2001).

For sub-jets with $\theta_v^{(j)} \lesssim \Delta\theta_{\text{sub}}^{(j)}$, we have $\delta T^{(j)} \ll t_{\text{dur}}$, because t_{dur} is about several tens of seconds. Then the bright pulses arising from these sub-jets are concentrated in the epoch $0 \lesssim T \lesssim t_{\text{dur}}$. On the other hand, for sub-jets with $\theta_v^{(j)} \gtrsim 0.1 r_{14}^{-1/2} (t_{\text{dep}}^{(j)}/20 \text{ sec})^{1/2}$, the second terms of the right hand sides of Eqs. (1) and (2) become larger than the first ones, so that

$T_{\text{start}}^{(j)}$ and $T_{\text{end}}^{(j)}$ may be much larger than t_{dur} for large $\theta_v^{(j)}$. Such smooth, long-duration, dim, and soft pulses make the tail emission of the prompt GRB.

Now we concentrate on the temporal structure of the tail emission. We assume that each sub-jet is not drastically different. Since $T_{\text{start}}^{(j)}$ and $T_{\text{end}}^{(j)}$ are much larger than t_{dur} , they are not affected by $t_{\text{dep}}^{(j)}$. Thus we may consider that all the sub-jets contributing to the tail emission emit simultaneously at a mean radius r_0 in the central engine frame. The end of the tail emission T_{tail} is determined by the angular size of the whole jet:

$$T_{\text{tail}} \sim (r_0/2c)(\Delta\theta_{\text{tot}} + \vartheta_{\text{obs}})^2 \sim 2 \times 10^2 r_{14} [(\Delta\theta_{\text{tot}} + \vartheta_{\text{obs}})/0.3]^2 \text{ sec} . \quad (5)$$

The tail flux at an observer time T is the superposition of the sub-jet emission with the pulse starting and ending time $T_{\text{start}}^{(j)} < T < T_{\text{end}}^{(j)}$. In other words, sub-jets with viewing angles between $\theta_T - \Delta\theta_{\text{sub}}$ and $\theta_T + \Delta\theta_{\text{sub}}$ contribute to the tail flux at a time T , where $\theta_T = (2cT/r_0)^{1/2} \sim 0.2r_{14}^{-1/2}(T/10^2 \text{ s})^{1/2}$ rad. Then we may calculate the number of these contributing sub-jets $N_{\text{sub}}(T)$ if the sub-jet distribution and observer's line of sight are given, and may also estimate the variance of the tail flux fluctuation as $1/\sqrt{N_{\text{sub}}(T)}$. While $N_{\text{sub}}(T)$ is sufficiently large, the tail light curve will be smooth. In the following, we actually draw the light curves of prompt GRB emission for various cases.

3.2. Example 1: Uniform jet

We first consider the uniformly distributed sub-jets. The number of sub-jets per unit solid angle is approximately given by $dN/d\Omega = N_{\text{tot}}/(\pi\Delta\theta_{\text{tot}}^2)$ for $\vartheta < \Delta\theta_{\text{tot}}$, where $\Delta\theta_{\text{tot}} = 0.25$ rad is adopted. The departure time of each sub-jet $t_{\text{dep}}^{(j)}$ is assumed to be homogeneously random between $t = 0$ and $t = t_{\text{dur}}$, where t_{dur} is the active time of the central engine measured in its own frame, and $t_{\text{dur}} = 20$ s is adopted. The central engine is assumed to produce $N_{\text{tot}} = 1000$ sub-jets. In this section, we assume that all the sub-jets have the same values of the following parameters: $\Delta\theta_{\text{sub}} = 0.02$ rad, $\gamma = 100$, $r_0 = 1.0 \times 10^{14}$ cm, $\alpha_B = -1$, $\beta_B = -2.3$, $h\nu'_0 = 5$ keV, and $A = \text{const}$. We call these a fiducial parameter set.

Figure 1 shows the results, where $\vartheta_{\text{obs}} = 0$ (red lines), $\Delta\theta_{\text{tot}}/2$ (green), $\Delta\theta_{\text{tot}}$ (blue), and $3\Delta\theta_{\text{tot}}/2$ (purple) are considered. One can see the entire behavior of bursts in the left panel of the figure. For the cases $\vartheta_{\text{obs}} < \Delta\theta_{\text{tot}}$, as expected, the bright pulses are observed in the period $0 \lesssim T \lesssim t_{\text{dur}} = 20$ sec, and subsequently the tail emission starts. However, when $\vartheta_{\text{obs}} = 3\Delta\theta_{\text{tot}}/2$, the whole jet is seen off-axis. Then the observed flux is lower than the other and the spectrum is softer, so that the event is observed as an X-ray flash (Yamazaki, Ioka, & Nakamura 2002, 2003, 2004a,b). In any cases, the tail emission is smooth. For $\vartheta_{\text{obs}} = 0$, the number of contributing sub-jets $N_{\text{sub}}(T)$ is approximately given by $N_{\text{sub}}(T) \approx$

$4\pi\theta_T\Delta\theta_{\text{sub}}(dN/d\Omega)$. For our adopted parameters, we derive $N_{\text{sub}}(T) \sim 2.6 \times 10^2 (T/10^2 \text{ s})^{1/2}$. It is sufficiently larger than unity, so that the tail light curve is smooth. Also in other cases ($\vartheta_{\text{obs}} \neq 0$), we obtain $N_{\text{sub}}(T) \gg 1$.

The decay index of the tail emission is about -4 when it is determined by the whole light curve (left panel of Fig 1). The effect of choosing the zero of time is essential in order to determine the decay index of the tail emission (Chincarini et al. 2005; Zhang et al. 2005). The right panel of Fig. 1 shows the same light curves as in the left panel but the time zero is shifted to the maximum of the last bright pulse. Then, the decay index of the tail emission ranges between -3 and -2 . Since we may consider that all the sub-jets emit simultaneously in the central engine frame for the tail emission, the behavior of the emission may be similar for a single, spherical, infinitesimally thin shell case. Then it is expected that The decay index of $-1 + \beta_B = -3.3$ is intermediate between those shown in the left and the right panel. This implies that the zero of time which gives us the index predicted by Kumar & Panaitescu (2000) lies between the onset of the burst and the last bright pulse.

3.3. Example 2: Power-law jet

In this subsection we consider the power-law sub-jet distribution, i.e., $dN/d\Omega = C$ for $0 < \vartheta < \vartheta_c$ and $dN/d\Omega = C(\vartheta/\vartheta_c)^{-2}$ for $\vartheta_c < \vartheta < \Delta\theta_{\text{tot}}$, where $\vartheta_c = 0.03$ rad and $\Delta\theta_{\text{tot}} = 0.3$ rad are adopted (Rossi, Lazzati, & Rees 2002; Zhang & Mészáros 2002; Toma, Yamazaki, & Nakamura 2005a,b). The normalization constant C is determined as $C = (N_{\text{tot}}/\pi\vartheta_c^2)[1 + 2\ln(\Delta\theta_{\text{tot}}/\vartheta_c)]^{-1}$. The departure time of each sub-jet $t_{\text{dep}}^{(j)}$ is again assumed to be homogeneously random between $t = 0$ and $t = t_{\text{dur}} = 20$ sec. The central engine is assumed to produce $N_{\text{tot}} = 350$ sub-jets.

First we assume that all the sub-jets have the fiducial parameters. Figure 2 shows the results for $\vartheta_{\text{obs}} = 0$ (red lines), $\Delta\theta_{\text{tot}}/2$ (green), $\Delta\theta_{\text{tot}}$ (blue), and $3\Delta\theta_{\text{tot}}/2$ (purple). Compared with the uniform jet case, the decay index is steeper because the power-law jet is dimmer in the outer region, i.e., the sub-jets are sparsely distributed near the periphery of the whole jet. For example, when $\vartheta_{\text{obs}} = 0$, the number of contributing sub-jets $N_{\text{sub}}(T)$ is calculated as $N_{\text{sub}}(T) \approx 4\pi\theta_T\Delta\theta_{\text{sub}}(dN/d\Omega) \sim 28 (T/100 \text{ s})^{-1/2}$. Then $N_{\text{sub}}(T)$ is a decreasing function of time, while in the uniform jet case $N_{\text{sub}}(T)$ increases with T until the end of time of the prompt emission. We note that some of the observed tails may be too shallow ($\sim T^{-3}$) to be consistent with the power-law jets ($\sim T^{-4}$).

As can be seen from the right panel of Fig. 2, a steepening break (from $\sim T^{-1}$ to $\sim T^{-4}$) occurs at about 35 sec and 100 sec after the last brightest pulse for $\vartheta_{\text{obs}} = \Delta\theta_{\text{tot}}/2$ and

$\vartheta_{\text{obs}} = \Delta\theta_{\text{tot}}$, respectively. This is because the power-law jet has a core region ($0 < \vartheta < \vartheta_c$), where sub-jets densely distributed compared with the outer region. Before photons emitted by the core arrive at the observer (i.e., $\theta_T \lesssim \vartheta_{\text{obs}}$), $N_{\text{sub}}(T)$ increases with T more rapidly than in the case of the uniform sub-jet distribution considered in § 3.2. Then, the light curve shows a shallow decay or even shows a rising part. After the photons arising from the core are observed, the sub-jet emission with viewing angles larger than $\sim \vartheta_c$ is observed. Then $N_{\text{sub}}(T)$ rapidly decreases with T and the observed flux suddenly drops. Therefore, a steepening break occurs at $\theta_T \sim \vartheta_{\text{obs}}$.

The left panel of Fig. 3 shows the dependence on the assumed parameters, especially on $\Delta\theta_{\text{sub}}$, γ , and r_0 (but still the same for all j). Instead, we fix the observer’s line of sight, $\vartheta_{\text{obs}} = 0$. The red line is the same as the red ones in Fig. 2 (the fiducial set). We also have the green ($\gamma = 400$), blue ($\Delta\theta_{\text{sub}} = 0.01$ rad), purple ($\gamma = 400$ and $\Delta\theta_{\text{sub}} = 0.01$ rad), and light blue lines ($r_0 = 0.2 \times 10^{14}$ cm) with the other parameters being fiducial. The duration of the bright epoch (before the tail emission) is determined by the active time of the central engine, t_{dur} , so that it does not depend on the sub-jet properties. When r_0 is small (the light blue line) the tail emission ends rapidly, while the end time of the tail emission T_{tail} does not depend on $\Delta\theta_{\text{sub}}$ and γ [see Eq. (5)]. When γ is large (green and purple lines) the asymptotic decay index is not altered, while the flux becomes dim because the relativistic beaming effect is large. When $\Delta\theta_{\text{sub}}$ is small (blue and purple lines), $\delta T^{(j)}$ is small [see Eq. (3)], so that $N_{\text{sub}}(T)$ decreases. Then the observed light curves remarkably reflect fluctuations of $N_{\text{sub}}(T)$.

4. Discussions

We have discussed the tail emission of the prompt GRB emission in the X-ray band using a multiple emitting sub-shell (inhomogeneous jet, sub-jets) model. The sub-shell emission with a large viewing angle causes a smooth, long-duration, dim, soft pulse and arrives later than the bright hard spikes. These components make the tail emission of the prompt GRB. Our practical calculations have confirmed that our inhomogeneous jet model well reproduces the observed smooth light curve of the tail emission.

Since the pulse duration is long for a large viewing angle, the local inhomogeneity is averaged and the smoothed tail is obtained. Then the global sub-jet distribution is important for the behavior of the tail. Therefore, the discrete multiple sub-jet model and the continuous surface model obtained by averaging sub-jets predict the same decay index. Some of the observed tails are not steep enough to be consistent with the power-law jet model. We also find that if there is a core, in which many emitting shells exist compared with other regions, the steepening break appears in the tail when the core is viewed off-axis.

A typical value of the viewing angle at an observer time T is $\theta_T \sim 0.2(T/10^2 \text{ s})^{1/2}$ rad, and then the peak energy, E_p , is about a few keV [see Eq. (4)]. Therefore, the spectral index in the X-ray band is given by the high-energy photon index $\beta_B \sim -2.3$, which is consistent with the observed photon index that ranges between 1.34 and 3.25 (average value is 2.28) (Nousek et al. 2005),

Important parameters that characterize our model are the number of sub-jets N_{tot} and the opening half-angle of the sub-jet $\Delta\theta_{\text{sub}}$. Given the sub-jet angular distribution, the value of N_{tot} is determined in order to reproduce the number of sub-jets along a line of sight, n_s , that ranges between about 10 and 10^2 because n_s corresponds to the number of bright pulses observed in usual long GRBs (Yamazaki, Ioka, & Nakamura 2004b). In our adopted parameters, the maximum of n_s is about 10 and 30 for uniform jet case (§ 3.2) and the power-law jet case (§ 3.3), respectively. On the other hand, the value of $\Delta\theta_{\text{sub}}$ is fairly uncertain. It is a common sense that $\Delta\theta_{\text{sub}}$ is larger than γ^{-1} because even if $\Delta\theta_{\text{sub}} \ll \gamma^{-1}$ initially, jet expands sideways and the asymptotic value of $\Delta\theta_{\text{sub}}$ is γ^{-1} . However, in principle, $\Delta\theta_{\text{sub}}$ could be even smaller than γ^{-1} e.g., if the offset collision of two shells is considered. If the observation will confirm the smoothness of the tail emission, the limits on $\Delta\theta_{\text{sub}}$ could be obtained.

In this paper, we have assumed that all sub-jets have the same intrinsic properties. Here we discuss the case of variable sub-jet properties. Power law sub-jet distribution is again considered. The right panel of Fig. 3 shows the result in which the value of $\gamma\nu_0^{(j)}$ is distributed randomly according to the log-normal distribution with an average of $\log(350 \text{ keV})$ and a logarithmic variance of 0.2, and the amplitude $A^{(j)}$ is determined so that the time averaged flux in the case of $\theta_v = 0$ satisfies $F \propto \xi(E_p)^2$, where the coefficient ξ is also assumed to obey a log-normal distribution with a logarithmic variance of 0.15 (Lloyd-Ronning & Ramirez-Ruiz 2002; Yonetoku et al. 2004; Liang, Dai, & Wu 2004). The green line corresponds to the fiducial parameter set of $\Delta\theta_{\text{sub}}^{(j)}$, $\gamma^{(j)}$, and $r_0^{(j)}$, while the blue line is for $\gamma^{(j)} = 300$ and $r_0^{(j)} = 3.0 \times 10^{14} \text{ cm}$ (Toma, Yamazaki, & Nakamura 2005b). The tail emission remains smooth, and the decay slope is almost unchanged except for the purple line, where the logarithmic variance of $\gamma\nu_0^{(j)}$ is changed into 0.8. The logarithmic variance of the log-normal distribution of $\gamma\nu_0^{(j)}$ and ξ is uncertain. If these parameters are large, the tail emission is more variable. The observed smoothness of the tail emission may constrain the distribution of these parameters.

We would like to thank T. Sakamoto, G. Sato, T. Takahashi, and D. Yonetoku for useful comments and discussions. This work was supported in part by a Grant-in-Aid for the 21st Century COE “Center for Diversity and Universality in Physics” and also by Grants-in-Aid for Scientific Research of the Japanese Ministry of Education, Culture, Sports, Science, and

Technology 09245 (R. Y.), 14047212 (T. N., K. I.), 14204024 (T. N.), and 17340075 (T. N.).

REFERENCES

- Band, D. L., et al. 1993, *ApJ*, 413, 281
- Burrows, D. N. et al. 2005, *Science* in press, (astro-ph/0506130)
- Campana, S. et al. 2005, *ApJ*, 625, L23
- Chincarini, G. et al. 2005, astro-ph/0506453
- Connaughton, V. 2002, *ApJ*, 567, 1028
- Giblin, T. W. et al. 1999, *ApJ*, 524, L47
- Granot, J., Piran, T., & Sari, R. 1999, *ApJ*, 513, 679
- Ioka, K., & Nakamura T. 2001, *ApJ*, 554, L163
- Kumar, P., & Panaitescu, A. 2000, *ApJ*, 541, L51
- Kumar, P., & Piran, T. 2000, *ApJ*, 535, 152
- Kumar, P. & Granot, J. 2004, *ApJ*, 591, 1075
- Lazzati, D. & Begelman, M. C. 2005, preprint (astro-ph/0502084)
- Liang, E. W., Dai Z. G., & Wu, X. F. 2004, 606, L29
- Lloyd-Ronning, N. M. & Ramirez-Ruiz, E. 2002, *ApJ*, 576, 101
- Nakamura, T. 2000, *ApJ*, 534, L159
- Nousek, J. A. et al. 2005, astro-ph/0508332
- Panaitescu, A., Mészáros, P., Gehrels, N., Burrows, D., & Nousek, J. 2005, astro-ph/0508340
- Rossi, E., Lazzati, D., & Rees, M. J. 2002, *MNRAS*, 332, 945
- Tagliaferri, G. et al. 2005, *Nature*, in press, (astro-ph/0506355)
- Toma, K., Yamazaki, R., & Nakamura, T. 2005a, *ApJ*, 620, 835
- Toma, K., Yamazaki, R., & Nakamura, T. 2005b, *ApJ*, in press (astro-ph/0504624)

- Woods, E. & Loeb, A. 1999, *ApJ*, 523, 187
- Yamazaki, R., Ioka, K., & Nakamura, T. 2002, *ApJ*, 571, L31
- Yamazaki, R., Ioka, K., & Nakamura, T. 2003, *ApJ*, 593, 941
- Yamazaki, R., Ioka, K., & Nakamura, T. 2004a, *ApJ*, 606, L33
- Yamazaki, R., Ioka, K., & Nakamura, T. 2004b, *ApJ*, 607, L103
- Yamazaki, R., Ioka, K., Takahara, F., Shibazaki, N. 2005, *PASJ*, 57, L11
- Yonetoku, D., Murakami, T., Nakamura, T., Yamazaki, R., Inoue, A. K., & Ioka, K. 2004, *ApJ*, 609, 935
- Zhang, B., & Mészáros, P. 2002, *ApJ*, 571, 876
- Zhang, B. et al., 2005, [astro-ph/0508321](#)

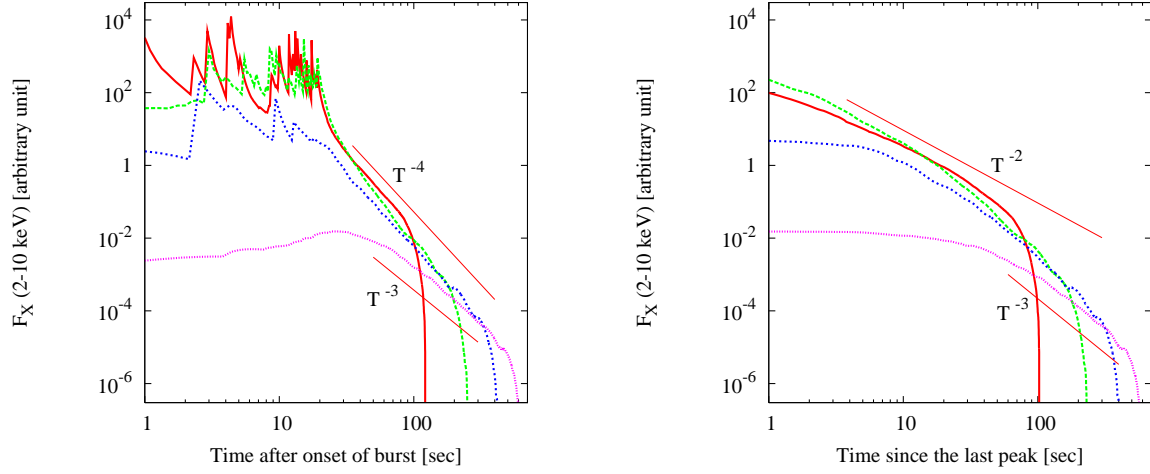


Fig. 1.— Examples of light curves of the prompt GRB emission calculated by the multiple emitting sub-shell model (multiple sub-jet model). The sub-jets are distributed uniformly. All sub-jets have the same intrinsic properties. Red, green, blue, and purple lines correspond the viewing angles of $\vartheta_{\text{obs}} = 0, \Delta\theta_{\text{tot}}/2, \Delta\theta_{\text{tot}},$ and $3\Delta\theta_{\text{tot}}/2,$ respectively. (left panel) The observer time is the time since the onset of the burst. (right panel) The observer time is the time since the last bright peak.

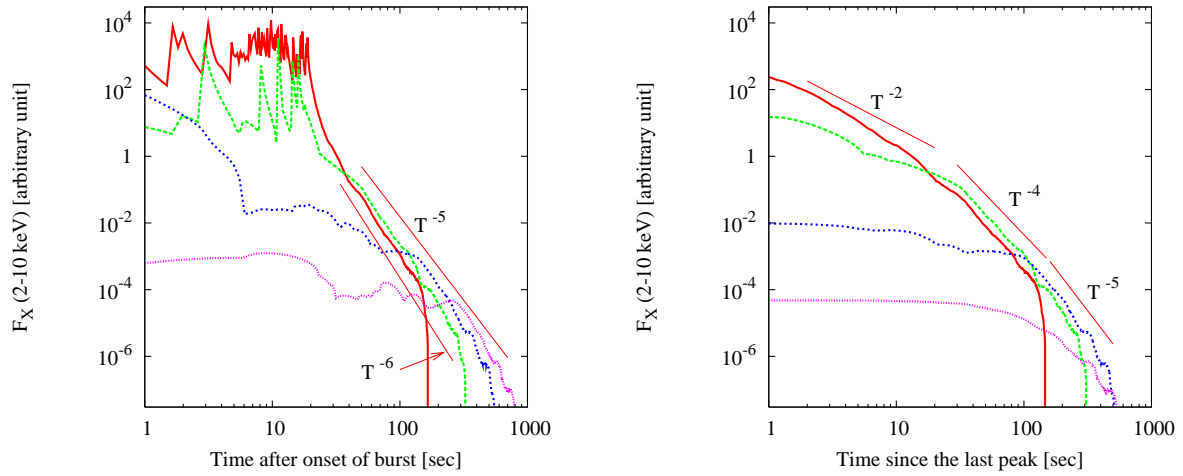


Fig. 2.— The same as Fig. 1 but for the power-law sub-jet distribution.

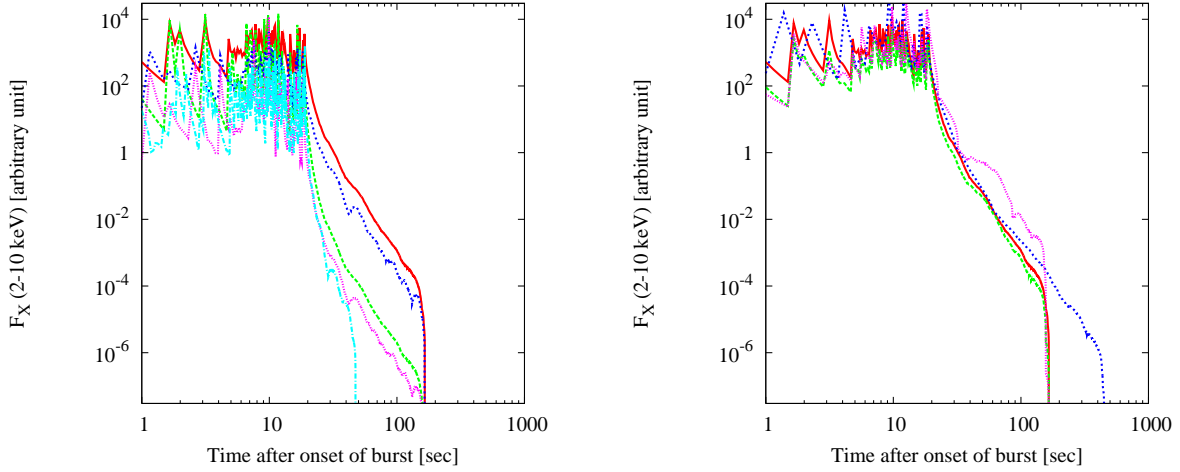


Fig. 3.— Comparison of light curves with different parameter sets of $\Delta\theta_{\text{sub}}$, γ , and r_0 for the power-law distribution. (left panel) Green ($\gamma = 400$), blue ($\Delta\theta_{\text{sub}} = 0.01$ rad), purple ($\gamma = 400$ and $\Delta\theta_{\text{sub}} = 0.01$ rad), and light blue lines ($r_0 = 0.2 \times 10^{14}$ cm) with the other parameters being fiducial, i.e., $\Delta\theta_{\text{sub}} = 0.02$ rad, $\gamma = 100$, and $r_0 = 1.0 \times 10^{14}$ cm. (right panel) The value of $\gamma\nu_0^{(j)}$ is distributed randomly according to the log-normal distribution with an average of $\log(350 \text{ keV})$ and a logarithmic variance of 0.2, and $A^{(j)}$ is determined so that the observed flux is proportional to ξE_p^2 for $\theta_v^{(j)} = 0$, where ξ is also assumed to obey a log-normal distribution with a logarithmic variance of 0.15. The green line corresponds to the fiducial parameter set of $\Delta\theta_{\text{sub}}$, γ , and r_0 , while the blue line is for $\gamma = 300$ and $r_0 = 3.0 \times 10^{14}$ cm. The purple line is for the case in which logarithmic variance of $\gamma\nu_0^{(j)}$ is changed into 0.8. Red lines of both panels are the same as the red ones in Fig. 2 (fiducial set). All lines have $\vartheta_{\text{obs}} = 0$.